Rizwan Ul Haq*, Z. H. Khan, W. A. Khan and Inayat Ali Shah

# Viscous Dissipation Effects in Water Driven Carbon Nanotubes along a Stream Wise and Cross Flow Direction

DOI 10.1515/ijcre-2016-0059

**Abstract:** Important physical models involving boundary layer occur in almost all internal and external aerodynamic formations. For many of these, the flow outside the boundary layer region may be determined into a large principal component and a small crosswise velocity. In this article, three-dimensional boundary-layer flow over a curved surface is treated for nanofluid under such a simplification. Based on strong thermal conductivity we have considered two same kinds but different shaped nanoparticle namely: Single Wall Carbon Nanotubes (SWCNT) and Multiple Wall Carbon Nanotubes (MWCNT) which are incorporated within the base fluid water. Mathematical model is constructed under the constraint of defined geometry and then transformed into the system of ordinary differential equations. These equations are solved numerically with the help of Runge Kutta (R-K) method with shooting technique. Influences of each physical parameter on velocity and temperature distribution are described through graphs. To analyze the drag and heat transfer at the surface we have plotted the skin friction coefficient and local Nusselt number. Flow behavior along the stream wise and cross direction is visualized through stream lines. It is found that viscous dissipation has same increasing effects along both *x*- and z-directions for temperature profile however, SWCNTs have comparatively higher skin friction and heat transfer rate at the surface as compare to the MWNTs.

**Keywords:** cross flow, dissipation effects, carbon nanotube, numerical solution

***Corresponding author: Rizwan Ul Haq,** Department of Mathematics, Quaid-i-Azam University, Islamabad 44000, Pakistan, E-mail: ideal_riz@hotmail.com; r.haq.qau@gmail.com
**Z. H. Khan,** Department of Mathematical, University of Malakand, Dir (Lower), Khyber Pakhtunkhwa, Pakistan
**W. A. Khan,** Departments of Basic Science, College of Engineering Majmaah University, Majmaah, 11952, Saudi Arabia
**Inayat Ali Shah,** Department of Mathematics, Islamia College Peshawar (CU), Khyber Pakhtunkhwa, Pakistan

## 1 Introduction

When a fluid flows over a plane surface, the curvature of the stream lines within the boundary layer differs from that of the free stream due to the pressure gradient normal to the direction of free-stream flow. The pressure in the boundary layer does not vary with distance from the surface, the boundary-layer flow must, because of its lower velocity, curve more sharply than the free-stream flow in order to balance this pressure gradient. The boundary layer velocity component normal to the direction of the free stream is known as the cross flow or the secondary flow. In these flows, the transverse motion is assumed to be fully developed. These flows can be found in many engineering situations like aerospace, mechanical, and wind flow phenomena.

Following the pioneering studies (Prandtl 1928; Blasius 1908) on the laminar flow over a flat plate with small viscosity, Jones (1947) studied the effects of sweepback on boundary-layer and separation and found that the independence of the cross flow and the axial flow is due to the result of the law of shearing stress used in the Navier-Stokes equations. Sears (1954) investigated the cross flow in the laminar boundary layer on an infinite swept wing where the pressure gradient in the free stream was normal to the leading edge. Sears calculated the resulting cross flow and showed in particular that the cross flow vanishes for the swept flat plate at zero angle of attack-that is, when the imposed pressure gradient vanished. Sowerby (1954) and Loos (1955) studied the secondary flows in a boundary layer. They selected incompressible laminar boundary layer over a flat plate for the simple case where the stream lines in the free flow have a parabolic shape. He found that no separation occurs, even when there is a strong adverse pressure gradient along the stream lines, so that in this instance the secondary flow has a favorable influence.

Hansen and Herzig (1956) studied cross flows in laminar incompressible boundary layers and analyzed the three-dimensional boundary-layer flow over a flat surface with a leading edge under main-flow streamlines. Tsung and Hansen (1967) obtained the similarity solutions to the

three-dimensional boundary layer equations in rectangular coordinates for a power law fluid. They found that the two components of the mainstream flow must differ by at most a multiplicative constant and the cross flow component may be generalized. Dwyer (1968) developed a method of calculating accurate solutions of the three-dimensional laminar boundary-layer equations. He applied this method to a problem that exhibits interesting cross flow phenomena, such as a flow reversal driven by cross flow convective terms and cross flow influences with zero free streams cross flow velocity. Klemp and Acrivos (1972) studied the problem of uniform flow past a parallel flat plate of finite length whose surface has a constant velocity directed opposite to that of the main stream. They found that, near the point of detachment, the solution has a self-similar form in this particular example. Later on, Klemp and Acrivos (1976) extended the range of $\lambda$ and found that the flow consists of three overlapping domains including an external uniform flow, a reverse flow and a cross flow. Hussaini, Lakin and Nachman (1987) investigated the problem of a boundary layer on a flat plate which has a constant velocity opposite in direction to that of the uniform mainstream. The boundary layers on the upstream-moving flat plate at zero incidences admit of the classical similarity transformation which reduces the relevant partial differential equations to the Blasius equation. Wang (1992) investigated uniform flow over a flat plate with an irregular leading edge. A similarity reduction to Blasius's equation for the three-dimensional flow is obtained in the context of boundary layer theory. The wall shear stress and also the boundary layer, displacement, and momentum thicknesses are found to be proportional to a common distribution function.

Weidman (1996) presented new solutions for laminar boundary layers with cross flow. He investigated five different problems related to cross flow within the confines of laminar boundary layer theory and reported new transverse flow solutions for some classical streamwise boundary layer flows which are expected to be of engineering interest. Later on, Weidman (1997) investigated uniform flow over a flat plate with an irregular leading edge. He obtained a similarity reduction to Blasius's equation for the three-dimensional flow and found that the wall shear stress and also the boundary layer, displacement, and momentum thicknesses are proportional to a common distribution function. Weidman, Kubitschek, and Brown (1997) determined similarity solution of the Prandtl boundary layer equations describing wall bounded flows and symmetric free-shear flows driven by rotational. An asymptotic analysis of the singular behavior of these two problems shows excellent comparison with the numerical results. Weidman, Kubitschek, and Davis (2006) studied the simultaneous effects of normal transpiration through and tangential movement of a semi-infinite plate. The flow was governed by a plate velocity parameter $\lambda$ and a transpiration parameter $\mu$. They found dual solutions and showed that the range of known dual solutions for zero transpiration increases with suction and decreases with blowing.

Nada (2009) studied the interactions of the effects of cross flow, buoyancy induced flow, orientation of the hot surface with respect to gravity, Reynolds numbers and Rayleigh numbers on heat transfer characteristics. For all surfaces orientations and for the entire ranges of Re and Ra, it was found that increasing the cross flow strength decreases the effective cooling of the surface. Fang and Lee (2009) extended the 3D boundary layers of wall-bounded flow configurations to the situations with span-wise cross moving boundary and free stream. They found that for the span-wise secondary boundary layer flow there is no flow separation for any wall cross moving velocity, which is different from the primary stream-wise boundary layers with a reverse flow. Bhattacharyya and Pop (2014) studied the dual nature of solutions for the forced convective boundary layer flow and heat transfer in a cross flow with viscous dissipation terms in the energy equation. They found that the dual solutions of the transformed similarity equations for velocity and temperature distributions exist for certain values of the moving parameter, Prandtl and Eckert numbers. Lee et al. (2014) presented new impingement heat transfer data to show the effects of impingement cross-flows on local, line-averaged, and spatially-averaged Nusselt numbers. They assumed constant impingement jet Reynolds number of 8,000. Current many authors present different ideas for nanofluid and heat transfer through various geometries that accomplish the wide attention at industrial level (Xue 2005; Rahman et al. 2016; Zeeshan, Majeed and Ellahi, 2016; Sheukhileslami and Ellahi, 2015; Ellahi, Hassan and Zeeshan, 2015a, 2015b; Sheikholeslami et al. 2015; Akbar, Raza and Ellahi, 2015; Hussain et al. 2016; Hayat et al. 2015; Hayat et al. 2015; Hayat et al. 2016).

In the view of above literature survey, main intention in this article is to discuss the boundary layer flow of nanofluid along the stream wise and cross direction. Mathematical model is constructed for curved surface having significant boundary layer effects. Two different shapes of nanoparticles (SWCNTs and MWCNTs) are incorporated within the base fluid (water). Dissipations effects are also considered along the stream wise and cross direction. Results are plotted for various for

emerging parameters for velocity, temperature, skin friction coefficient and local Nusselt number.

## 2 Mathematical modeling

In the case of yawed infinite wing, the problem of cross flow within the boundary layer has attained much intention because of its wide range of application. For this, we consider a 3-D constant (stream wise and cross) flow of nanofluid over a heated flat surface moving with the constant velocity $-\lambda U$ into and out of the origin located at $x=0$, where × is the coordinate measured along the flat surface, $\lambda$ is a dimensionless constant (say, moving parameter), and $U$ is the constant velocity of the outer flow (See Figure 1). It is assumed that the constant temperature of the plate is $T_w$, while the constant temperature of the ambient stream is $T_\infty$. It is also assumed that the cross-flow is of infinite extent in the span wise direction and so the assessment of this framework it is fully-established. As the developing equations: momentum and energy equations are free from the variable involved in coordinate $z$, so that the boundary layer equations accomplished the relations define for nanofluid can be written as (see Weidman 1996).

$$\frac{\partial u}{\partial x}+\frac{\partial v}{\partial y}=0, \tag{1}$$

$$u\frac{\partial u}{\partial x}+v\frac{\partial u}{\partial y}=\frac{\mu_{nf}}{\rho_{nf}}\frac{\partial^2 u}{\partial y^2}, \tag{2}$$

$$u\frac{\partial w}{\partial x}+v\frac{\partial w}{\partial y}=\frac{\mu_{nf}}{\rho_{nf}}\frac{\partial^2 w}{\partial y^2}, \tag{3}$$

$$u\frac{\partial T}{\partial x}+v\frac{\partial T}{\partial y}=\alpha_{nf}\frac{\partial^2 T}{\partial y^2}+\frac{\mu_{nf}}{(c_p\rho)_{nf}}\left(\left(\frac{\partial u}{\partial y}\right)^2+\left(\frac{\partial w}{\partial y}\right)^2\right), \tag{4}$$

Since the present phenomena addresses the boundary layer flow with stream wise and cross direction therefore the boundary conditions for velocities and temperature at wall are define as,

$$\begin{aligned} &u=-\lambda U,\ v=0,\ w=0,\ T=T_w \text{ at } y=0,\\ &u=U,\ w=W_0,\ T=T_\infty \text{ as } y\to\infty, \end{aligned} \tag{5}$$

In the above system of equations, $u$, $v$, and $w$ are the velocity components along $x$, $y$, and $z$-*axis*, respectively. Here, $y$ is the normal coordinate in the plane of the flow, $z$ is the spanwise coordinate in the direction of the transverse flow, $W_O$ is the transverse velocity at the origin (e. g. $w=W_0$ at $x=0$ for $y>0$). Since the movement of the plate depends on $\lambda$. When $(\lambda<0)$, plate moves out of the origin $x=0$ and for $\lambda>0$ the plate moves into the origin. Furthermore, temperature of the nanofluid is defined as $T$, $\alpha_{nf}$ is the thermal diffusivity of nanofluid, $\rho_{nf}$ is the density of nanofluid and $\mu_{nf}$ is the thermal diffusivity of nanofluid defined as:

$$\left.\begin{aligned} &\mu_{nf}=\frac{\mu_f}{(1-\phi)^{2.5}},\ \nu_{nf}=\frac{\mu_{nf}}{\rho_{nf}},\rho_{nf}=(1-\phi)\rho_f+\phi(\rho)_s,\\ &\alpha_{nf}=\frac{k_{nf}}{(\rho C_p)_{nf}},(\rho C_p)_{nf}=(1-\phi)(\rho C_p)_f+\phi(\rho C_p)_s\\ &\frac{k_{nf}}{k_f}=\frac{1-\phi+2\phi\left(\frac{k_{CNT}}{k_{CNT}-k_f}\right)\ln\left(\frac{k_{CNT}+k_f}{k_{CNT}}\right)}{1-\phi+2\phi\left(\frac{k_f}{k_{CNT}-k_f}\right)\ln\left(\frac{k_{CNT}+k_f}{k_{CNT}}\right)}, \end{aligned}\right\} \tag{6}$$

The expression of effective thermal conductivity $k_{nf}/k_f$ is introduced by Xue (2005) that us based on Maxwell theory compensate nanotubes with large axial ratio and influence of space distribution on CNTs. where $\phi$ is the nanoparticle fraction, $(\rho C_p)_{nf}$ is the effective heat capacity of a nanoparticle, $k_{nf}$ is the thermal conductivity of nanofluid, $k_f$ and $k_s$ are the thermal conductivities of the base fluid and nanoparticle, respectively, $\rho_f$ and $\rho_s$ are the densities of the base fluid and nanoparticle, respectively.

By introducing the following transformation,

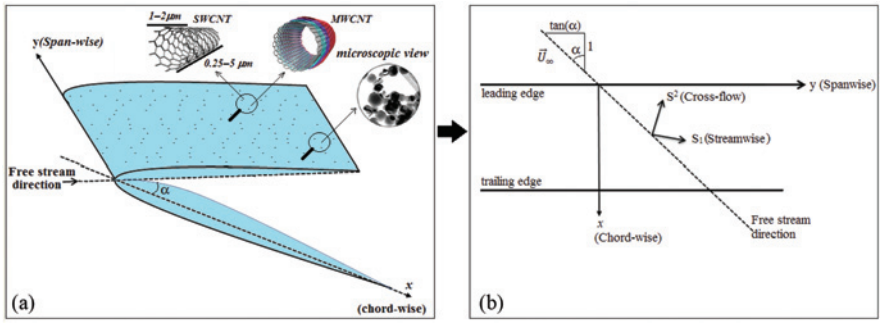


**Figure 1:** Illustration of the free-stream velocity $\vec{U}_\infty$, chord-wise direction-$x$, and span-wise direction $y$ for the swept-wing flow; $\alpha$ is the sweep angle.

$$\eta = \sqrt{\frac{U}{2xv_f}},\ \psi = \sqrt{2xUv_f} f(\eta),$$
$$w = W_0 g(\eta),\ \theta(\eta) = \frac{T - T_\infty}{T_w - T_\infty}. \tag{7}$$

In the above expression $\psi$ is the stream function, whereas $u = \partial\psi/\partial y$ and $v = -\partial\psi/\partial x$, and $\eta$ is the similarity variable. Making use of Eq. (7) in Eqs. (1) – (4). Equation (1) is identically satisfied while Eqs. (2)-(4) take the following form,

$$\frac{1}{(1-\phi)^{2.5}\left(1-\phi+\phi\frac{\rho_s}{\rho_f}\right)} f''' + ff'' = 0, \tag{8}$$

$$\frac{1}{(1-\phi)^{2.5}\left(1-\phi+\phi\frac{\rho_s}{\rho_f}\right)} g'' + fg' = 0, \tag{9}$$

$$\frac{(k_{nf}/k_f)}{\mathrm{Pr}}\theta'' + \left(1-\phi+\phi\frac{(\rho)_s(C_p)_s}{(\rho)_f(C_p)_f}\right) f\theta' + \frac{1}{(1-\phi)^{2.5}}\left(Ec_1 f''^2 + Ec_2 g'^2\right) = 0, \tag{10}$$

Corresponding boundary condition defined in Eq. (7), will takes the following form,

$$f(0) = 0,\ f'(0) = -\lambda,\ g(0) = 0,\ \theta(0) = 1,$$
$$f'(\eta) \to 1,\ g(\eta) \to 1,\ \theta(\eta) \to 0 \text{ as } \eta \to \infty \tag{11}$$

In the above last three equations, prime ($'$, $''$, $'''$) denotes the first, second and third derivative with respect to $\eta$, $\mathrm{Pr} = \nu_f/\alpha_f$ is the Prandtl number, $Ec_1 = U^2/c_p(T_w - T_\infty)$ and $Ec_2 = {W_0}^2/c_p(T_w - T_\infty)$ are the Eckert numbers.

Expressions for skin friction coefficients along the stream wise $C_{fx}$ and cross flow $C_{fz}$ along × and $z$-direction, respectively, are defined as:

$$C_{fx} = \frac{\tau_{wx}}{\rho_f U_{wx}^2} = \frac{\mu_{nf}\left(\frac{\partial u}{\partial y}\right)_{y=0}}{\rho_f U^2} = \frac{1}{\sqrt{2\mathrm{Re}_x}(1-\phi)^{2.5}} f''(0),$$
$$C_{fz} = \frac{\tau_{wz}}{\rho_f W_0^2}\frac{\mu_{nf}\left(\frac{\partial w}{\partial z}\right)_{z=0}}{\rho_f W_0^2} = \frac{1}{\sqrt{2\mathrm{Re}_x}(W_0/U)(1-\phi)^{2.5}} g'(0). \tag{12}$$

In the above Eq. (12), $\tau_{wx} = \mu_{nf}(\partial u/\partial y)$ and $\tau_{wz} = \mu_{nf}(\partial w/\partial y)$are the wall shear stresses along the stream wise direction and along the transverse direction, respectively. Where, $\mathrm{Re}_x = Ux/\nu$ is the local Reynolds number.

The Dimensionless form of local Nusselt number $Nu_x$ is defined as:

$$Nu_x = \frac{xq_w}{k_f(T_w - T_\infty)} = \frac{x\left(-k\frac{\partial T}{\partial y}\right)_{y=0}}{k_f(T_w - T_\infty)} = -\frac{(k_{nf}/k_f)\theta'(0)}{\sqrt{\mathrm{Re}_x/2}}. \tag{13}$$

Here $q_w$ is the heat flux from the flat plate.

# 3 Numerical method

The system of coupled nonlinear differential equations (8)-(10) along with the boundary conditions defined in Eq. (11) are tackled via numerically technique. Since the present mathematical model comprises the two point boundary value problem (BVP) so we apply Runge–Kutta–Fehlberg (RKF) method to achieve the realizable results. The step size is taken as $\Delta\eta = 0.01$ and the procedure for RKF method is repeated until we get the asymptotically convergent results within a tolerance level of $10^{-6}$. All these working schemes are assimilated in the computational software MATLAB 13.

# 4 Results and discussion

In order to analyze the nanofluid flow behavior, results are plotted against the unknown function of velocities $f'(\eta)$ and $g(\eta)$ along stream wise and cross flow directions, respectively. Similarly, to detect the temperature distribution against each physical parameter, results are plotted for $\theta(\eta)$. Thermo-physical properties of base fluid and CNT are taken from experimental data and utilized for present phenomena (see Table 1). To determine the heat transfer at the surface numerical results are determine in Table 2 for local Nusselt number for various values of nanoparticle volume fraction.

**Table 1:** Thermophysical properties of base fluid and nanoparticles (Hussain et al., 2016).

| Physical properties | Base fluid (Water) | Nanoparticles | |
|---|---|---|---|
| | | SWCNT | MWCNT |
| $\rho$(kg/m$^3$) | 997 | 2,600 | 1,600 |
| $C_p$(J/kg K) | 4,179 | 425 | 796 |
| $k$(W/m K)k | 0.613 | 6,600 | 3,000 |
| Pr | 6.2 | | |

Numerical values are calculated for Nusselt number against each physical parameter in Table 2. Main emphasis that covers the two important features of the present model, first one is to check the flow behavior of nanofluid along stream wise and cross direction and other is to discuss the heat transfer enhancement for water in the presence of single and multiple wall carbon nanotubes. In Figure 2(a) and 2(b), results are plotted for velocities along stream wise and cross flow. It can be observed that,

**Table 2:** Numerical values of local Nusselt number for various values of emerging parameters.

| | | | SWCNTs | | | MWCNTs |
|---|---|---|---|---|---|---|
| | | | | | | $Ec_1 = Ec_2 = 0.2$ |
| $\phi \downarrow$ | $\lambda = -0.15$ | $\lambda = 0$ | $\lambda = 0.15$ | $\lambda = -0.15$ | $\lambda = 0$ | $\lambda = 0.15$ |
| 0 | 0.451262 | 0.256448 | 0.048202 | 0.451262 | 0.256448 | 0.048202 |
| 0.1 | 0.927370 | 0.655411 | 0.364184 | 0.902970 | 0.632396 | 0.340605 |
| 0.2 | 1.271888 | 0.947781 | 0.603869 | 1.243406 | 0.917931 | 0.567934 |
| | | | | | | $Ec_2 = \lambda = 0.2$ |
| $\phi \downarrow$ | $Ec_1 = 0$ | $Ec_1 = 0.1$ | $Ec_1 = 0.2$ | $Ec_1 = 0$ | $Ec_1 = 0.1$ | $Ec_1 = 0.2$ |
| 0 | 0.172856 | 0.076144 | −0.02057 | 0.172856 | 0.076144 | −0.02057 |
| 0.1 | 0.568870 | 0.415656 | 0.262442 | 0.521027 | 0.379657 | 0.238287 |
| 0.2 | 0.905913 | 0.694796 | 0.48368 | 0.813661 | 0.628973 | 0.444284 |
| | | | | | | $Ec_1 = \lambda = 0.2$ |
| $\phi \downarrow$ | $Ec_1 = 0$ | $Ec_1 = 0.1$ | $Ec_1 = 0.2$ | $Ec_1 = 0$ | $Ec_1 = 0.1$ | $Ec_1 = 0.2$ |
| 0 | 0.113754 | 0.046593 | −0.02057 | 0.113754 | 0.046593 | −0.02057 |
| 0.1 | 0.475239 | 0.368841 | 0.262442 | 0.434634 | 0.336461 | 0.238287 |
| 0.2 | 0.776897 | 0.630288 | 0.48368 | 0.700796 | 0.57254 | 0.444284 |

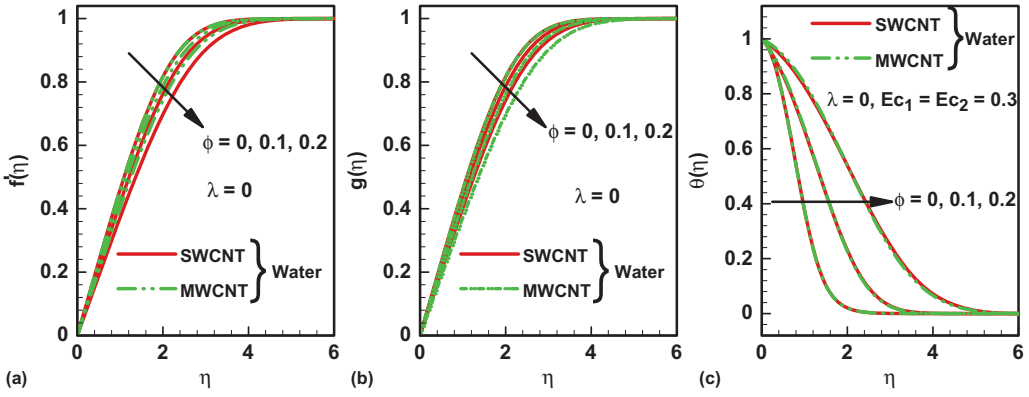


**Figure 2:** Variation of (a) $f'(\eta)$ (b) $g(\eta)$ (c) $\theta(\eta)$ for various values of nanoparticle volume fraction.

because of high density of SWCNTs result obtained for velocity profile are greater as compare to the MWCNTs. It can be further observed that increase of nanoparticle volume fraction gives decreasing behavior for velocities along stream wise and cross flow directions. Then dynamic of nanofluid flow analysis is based on density, that is when the nanoparticles will be added within the base fluid then density of whole mixture will become more thick and it will reduce the flow motion of nanofluid. Consequently, it will resist the nanofluid motion at the surface of the stretching plate. Similarly the temperature distribution of present analysis is based on the thermal conductivity of nanoparticles and base fluid. As we can observe from Table 1, that the thermal conductivity of SWCNT's is comparatively high as compare to MWCNT's. So, the temperature profile of water based SWCNT's is greater than water based MWCNT's. Further we can observed that temperature distribution $\theta(\eta)$ is increasing function of nanoparticle volume fraction $\phi$. Throughout the analysis it is found that velocity and thermal boundary layer is getting increase by incorporating the nanoparticles.

In Figure 3, results are plotted for velocity profiles along stream wise and cross flow directions for various values of $\lambda$. As we have mentioned before that, for the movement of the plate depends on $\lambda$ in such a way that for $\lambda < 0$ the plate moves out of the origin ($x = 0$), for $\lambda > 0$ the plate moves into the origin and for $\lambda = 0$ plate will remain in static position. Influence of $\lambda$for both stream wise and cross flow directions give similar decreasing g behavior. Effects of $\lambda$ on temperature distribution are plotted in Figure 4(a). As $\lambda = 0.3$ the plate moves into the origin so based on that analysis maximum heat will transfer at the vicinity of the hot surface. However for $\lambda = -0.4$ the plate moves out of the origin so less heat will transfer far from the hot surface. Combine effects of

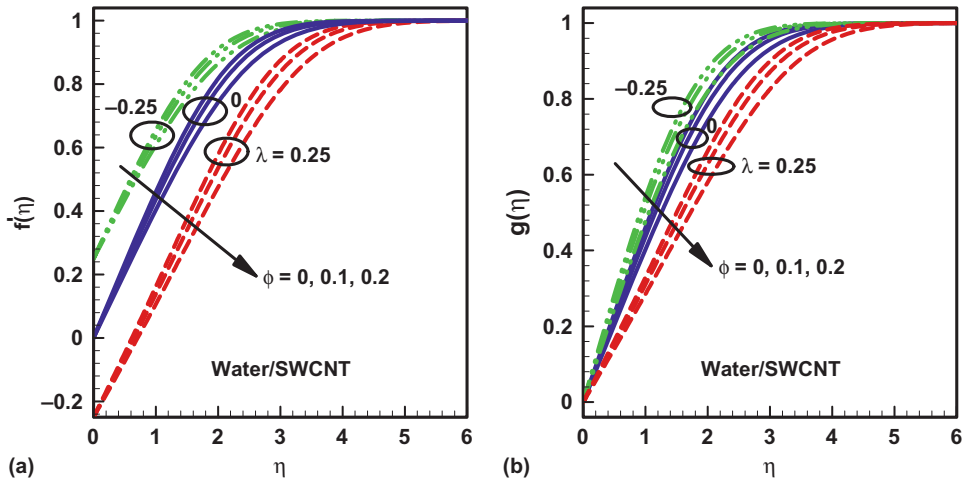


**Figure 3:** Variation of (a) $f'(\eta)$, (b) $g(\eta)$ for various values of $\lambda$ and nanoparticle volume fraction $\phi$.

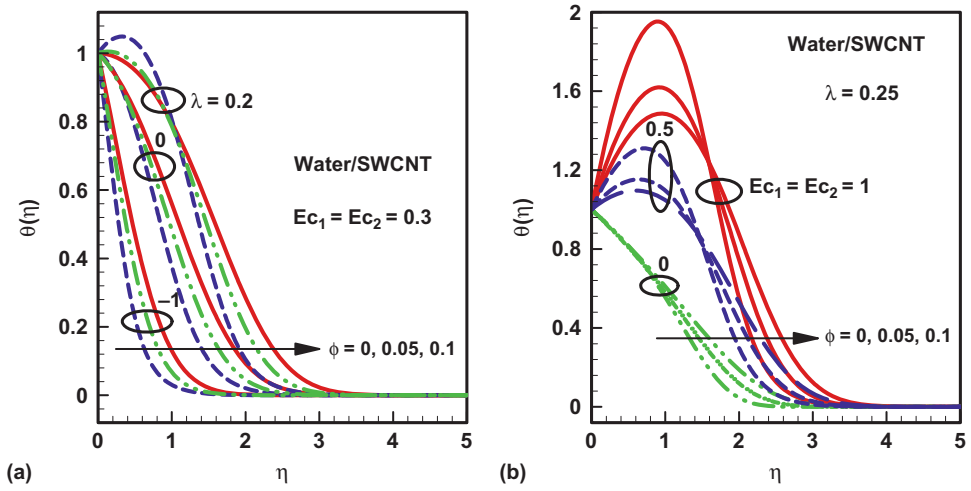


**Figure 4:** Variation of temperature profile $\theta(\eta)$ for various values of $\lambda$, $Ec_1 = Ec_2$ and nanoparticle volume fraction $\phi$.

$Ec_1$ and $Ec_2$ on temperature profile are plotted in Figures 4(b) and 5. Since viscous dissipation is the ratio of inertial forces to enthalpy generation, so increase in the inertial forces will increase the temperature profile. Results plotted in Figures 4(b) and 5, reflects the same increasing behavior for temperature profile against $Ec_1$ and $Ec_2$. Further it can be analyze that, increase in the nanoparticle volume fraction switched the behavior of temperature profile at the vicinity of the surface for increasing values of both $Ec_1$ and $Ec_2$. This state of switching the behavior of temperature profile is more dominant for large values of each Eckert number. Through this analysis it is further observed the temperature profile is an increasing function of nanoparticle volume fraction.

Figure 6, describes the combine effects of $\lambda$ and $\phi$ at the surface (skin friction coefficient) along the stream wise and cross flow directions. It can be observed that behavior of the skin friction coefficients along both stream wise and cross flow directions are relatively same increasing behavior for nanoparticle volume fraction. For $(\lambda < 0)$ when the plate moves away from the origin $(x = 0)$ then the behavior of skin friction coefficient along the stream wise direction shows higher profile as compare to $(\lambda > 0)$ when the plate moves into the origin. Further, it can be observed that when $(\lambda = 0)$ plate will remain in static position so we can observe the highest skin friction along the stream wise direction. Figure 6(b) depicts that the skin friction along cross flow gives decreasing behavior with increasing values of $\lambda$. As we have mentioned before, when the plate will moves toward the origin $(\lambda > 0)$ then higher heat will transfer from wall to the fluid and gradually

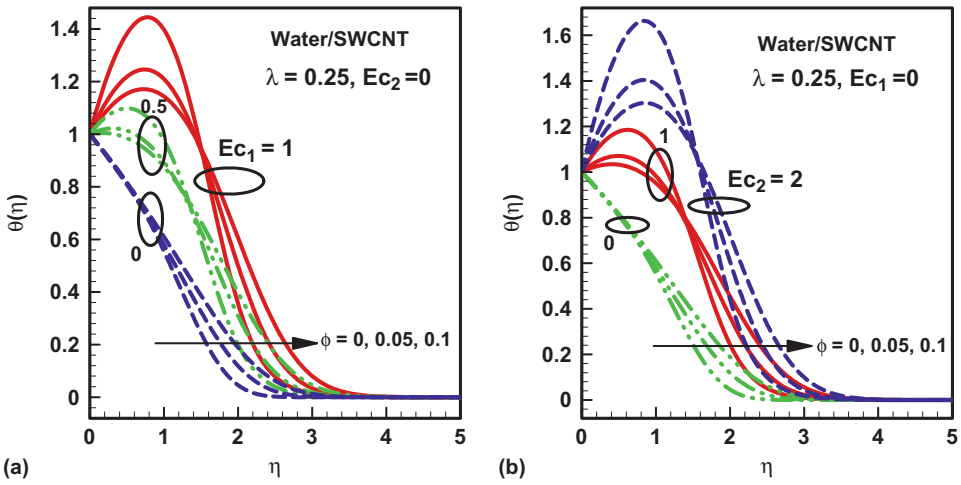


**Figure 5:** Variation of temperature profile $\theta(\eta)$ for various values of $\lambda$, $Ec_1$, $Ec_2$ and nanoparticle volume fraction $\phi$.

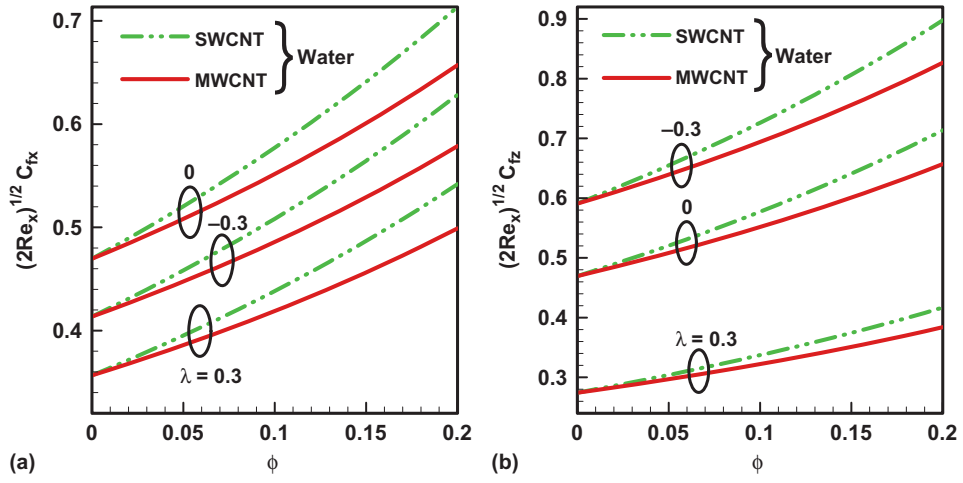


**Figure 6:** Variation of skin friction for various values of $\lambda$ (a) $\sqrt{2\mathrm{Re}_x}C_{fx}$, (b) $\sqrt{2\mathrm{Re}_x}C_{fz}$.

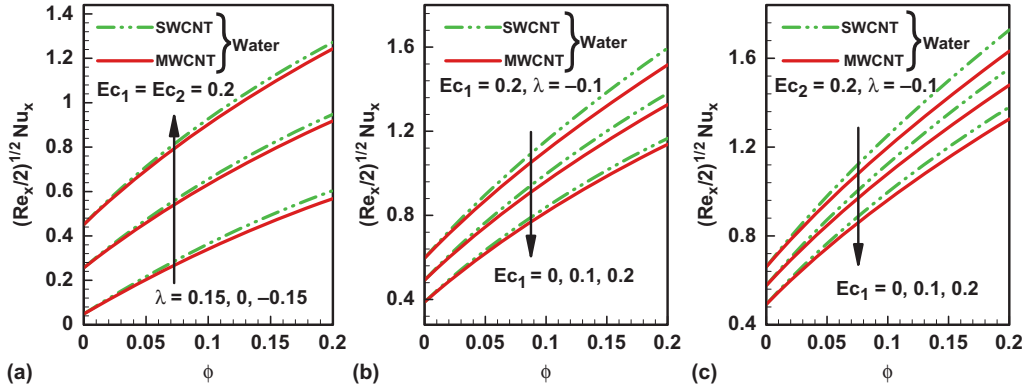


**Figure 7:** Variation of local Nusselt number for various values of (a) $\lambda$, (b) $Ec_2$ (c) $Ec_1$.

when sheet will move away from the wall then the effects of heat transfer will loss due to less energy transfer among the molecules (See Figure 7(a)). Viscus dissipation along $Ec_1$ and $Ec_2$ gives the same increasing results for local Nuseelt numer (See Figure 7(a)). In Figure 7, because of high thermal conductivity of SWCNTs provides the higher heat transfer rate at the surface as compare to the MWCNTs. Flow behavior for

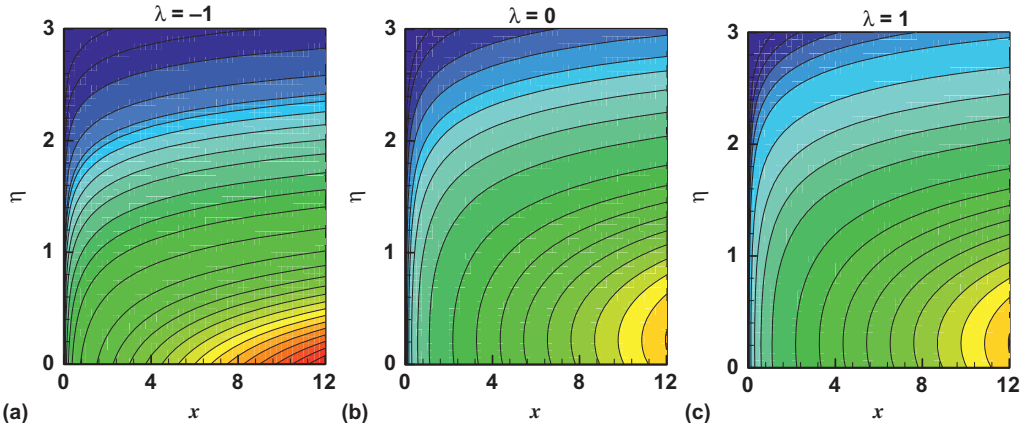


**Figure 8:** Stream flow behavior for various values of $\lambda$.

various values of $\lambda$ can be predicted through stream lines plotted in Figure 8.

## 5 Conclusion

In this study we have discussed the three dimensional boundary layer flow of nanofluid along steam wise and cross direction. We have further analyzed the heat transfer difference in the water by incorporating the SWCNT and MWCNT. Dissipation effects are also considered along $x$- and $z$-directions. Important results are constructed in results and discussion section and dig out the following key finding.

- Increase in the nanoparticle volume fraction will decrease the velocity profiles along $x$- and z-directions. However, nanoparticle volume fraction enhanced the temperature distribution.
- Increase in the $\lambda$ assist the same decreasing behavior for velocity profiles along $x$- and z-directions and results are quit opposite for temperature profile.
- Viscous dissipation along $x$- and z-directions has same increasing effects on temperature profile.
- Increase in the nanoparticle volume fraction provides the enhancement in the skin friction and heat transfer rate at the surface.
- SWCNTs have comparatively higher skin friction and heat transfer rate at the surface as compare to the MWNTs.

## References

1. Akbar, N.S., Raza, M., Ellahi, R., 2015. Influence of induced magnetic field and heat flux with the suspension of carbon nanotubes for the peristaltic flow in a permeable channel. Magnetism and Magnetic Materials 381, 405–415.
2. Bhattacharyya, K., Pop, I., 2014. Heat transfer for boundary layers with cross flow. Chinese Physics B 23(2), 024701–024706.
3. Blasius, H., 1908. Grenzschichten in Fl¨ussigkeiten mit kleiner Reibung. Zeitschrift für Angewandte Mathematik und Physik 56, 1–37.
4. Dwyer, H.A., 1968. Solution of a three-dimensional boundary-layer flow with separation. AIAA Journal 6(7), 1336–1342.
5. Ellahi, R., Hassan, M., Zeeshan, A., 2015a. Shape effects of nanosize particles in Cu-$H_20$ nanofluid on entropy generation. International Journal of Heat and Mass Transfer 81, 449–456.
6. Ellahi, R., Hassan, M., Zeeshan, A., 2015b. Study on magnetohydrodynamic nanofluid by means of single and multi-walled carbon nanotubes suspended in a salt water solution. IEEE Transactions on Nanotechnology, 14(4), 726–734.
7. Fang, T., Lee, C-F.F., May 2009. Three-dimensional wall-bounded laminar boundary layer with span-wise cross free stream and moving boundary. Acta Mechanica 204(3–4), 235–248.
8. Hansen, A.G, Herzig, H.Z., 1956. Cross flows in laminar incompressible boundary layers. NACA Technical Note 3651.
9. Hayat, T., Hussain, T., Shehzad, S.A., Alsaedi, A., 2015. Flow of Oldroyd-B fluid with nanoparticles and thermal radiation. Applied Mathematics and Mechanics 36(1), 69–80.
10. Hayat, T., Muhammad, T., Ahmad, B., Shehzad, S.A., 2016. Impact of magnetic field in three-dimensional flow of Sisko nanofluid with convective condition. Journal of Magnetism and Magnetic Materials 413, 1–8.
11. Hayat, T., Muhammad, T., Shehzad, S.A., Alhuthali, M.S., Lu, J., 2015. Impact of magnetic field in three-dimensional flow of an Oldroyd-B nanofluid. Journal of Molecular Liquids 212, 272–282,
12. Hussain, S.T., Ul Haq, R., Khan, Z.H., Nadeem, S., 2016. Water driven flow of carbon nanofluid nanotubes in a rotating channel. Journal of Molecular Liquids 214, 136–144.
13. Hussaini, M.Y., Lakin, W.D., Nachman, A., 1987. On similarity solutions of a boundary layer problem with an upstream moving wall. SIAM Journal on Applied Mathematics 47, 699–709.
14. Jones, R.T., 1947. Effects of sweepback on boundary-layer and separation, Rep. Nat. Adv. Comm. Aer., Washington No. 884.

15. Klemp, J.B., Acrivos, A., 1972. A method for integrating the boundary-layer equations through a region of reverse flow. Journal of Fluid Mechanics 53, 177–191.
16. Klemp, J.B., Acrivos, A.A., 1976. A moving-wall boundary layer with reverse flow. Journal of Fluid Mechanics 76, 363–381.
17. Lee, J., Ren, Z., Ligrani, P., Hee Lee, D., Fox, M.D., Moon, H.K., 2014. Cross-flow effects on impingement array heat transfer with varying jet-to-target plate distance and hole spacing. International Journal of Heat and Mass Transfer 75, 534–544.
18. Loos, H.G., 1955. A simple laminar boundary layer with secondary flow. Journal of the Aeronautical Sciences 22, 35–40.
19. Nada, S.A., 2009. Buoyancy and cross flow effects on heat transfer of multiple impinging slot air jets cooling a flat plate at different. Heat and Mass Transfer/Waermeund Stoffuebertragung 45(8), 1083–1097.
20. Prandtl, L., 1928. Uber Fl¨ussigkeitsbewegung bei sehr kleiner Reibung, Verh. III. Int. Math. Kongr., Heidelberg, 484–491. Teubner, Leipzig. In English see 'Motion of fluids with very little viscosity'.
21. Rahman, S.U., Ellahi, R., Nadee, S., Zaigham Zia, Q.M., 2016. Simultaneous effects of nanoparticles and slip on Jeffery fluid through trapered artery with mild stenosis. Journal of Molecular Liquid 218, 484–493.
22. Sears, W.R., 1954. Boundary layers in three-dimensional flow. Applied Mechanics Reviews 7, 281–285.
23. Sheikholeslami, M., Ganji, D.D., Javed, M.Y., Ellahi, R., 2015. Effect of thermal radiation on nanofluid flow and heat transfer using two phase model. Journal of Magnetism and Magnetic Materials 374, 36–43.
24. Sheukhileslami, M., Ellahi, R., 2015. Electrohydrodynamic nanofluid hydrothermal treatment in an enclosure with sinusoidal upper wall. Applied Sciences 5, 294–306.
25. Sowerby, L., 1954. Secondary flow in a boundary layer. Rep. Aero. Res. Coun. Lond., No. 16832.
26. Tsung, Y.N., Hansen, A.G., December 1967. Similarity solution of a class of laminar three-dimensional boundary layer equations of power law fluids. International Journal of Non-Linear Mechanics 2(4), 373–385.
27. Wang, C.Y., 1992. The boundary layers due to shear flow over a still fluid. Physics of Fluids A: Fluid Dynamics 4, 1304.
28. Weidman, A., 1996. New solutions for laminar boundary layers with cross flow. Zeitschrift für angewandte Mathematik und Physik ZAMP 48(2), 341–356.
29. Weidman, P.D., 1997. Blasius boundary layer flow over an irregular leading edge. Physics of Fluids 9(5), 1997.
30. Weidman, P.D., Kubitschek, D.G., Brown, S.N., 1997. Boundary layer similarity flow driven by power-law shear. Acta Mechanica 120(1–4), 199–215.
31. Weidman, P.D., Kubitschek, D.G., Davis, A.M.J., 2006. The effect of transpiration on self-similar boundary layer flow over moving surfaces. International Journal of Engineering Science 44(11–12), 730–737.
32. Xue, Q., 2005. Model for thermal conductivity of carbon nanotube based composites. Physica B: Condensed Matter 368, 302–307.
33. Zeeshan, A., Majeed, A., Ellahi, R., 2016. Effect of magnetic dipole on viscous ferro-fluid past a stretching surface with thermal radiation. Journal of Molecular Liquids 215, 549–554.